Equilibrium characteristics of semiflexible polymer solutions near probe particles

Venkat Ganesan,* Landry Khounlavong, and Victor Pryamitsyn
Department of Chemical Engineering, The University of Texas at Austin, Austin, Texas 78712, USA
(Received 16 August 2008; published 13 November 2008)

We present a numerical analysis of the mean-field theory for the structure of semiflexible polymer solutions near spherical surfaces, and use the framework to study the depletion characteristics of semiflexible polymers near colloids and nanoparticles. Our results suggest that the depletion characteristics depend sensitively on the polymer concentrations, the persistence lengths, and the radius of the particles. Broadly, two categories of features are identified based on the relative ratios of the persistence lengths to the correlation length of the polymer solution. For the limit where the correlation length is larger than the persistence length, the correlation length proves to be the critical length scale governing both the depletion thickness and the curvature effects. In contrast, for the opposite limit, the depletion thickness and the curvature effects are dependent on a length scale determined by an interplay between the persistence length and the correlation length. This leads to nontrivial (numerical) scaling laws governing the concentration and radii dependence of the depletion thicknesses. Our study also highlights the manner by which the preceding features rationalize the parametric dependencies of insertion free energies of small probes in semiflexible polymer solutions.

DOI: 10.1103/PhysRevE.78.051804 PACS number(s): 61.25.he, 61.20.−p, 82.70.Dd

Recent developments in experimental tools such as microrheology and particle tracking measurements have led to considerable interest in quantifying the equilibrium and dynamical characteristics in mixtures of polymer solutions and probe particles [1–5]. Motivation for a fundamental understanding of such issues also arise from numerous biological phenomena involving the behavior of globular proteins in crowded macromolecular environments [6,7]. Fundamental to such applications is an understanding and knowledge of the structure of polymer solutions around the spherical probes. For instance, microrheology experiments have demonstrated that to render a quantitative equivalence between the microrheology and macrorheology measurements, one needs to account for the mechanical properties of polymer depletion layer around the particles [1–4]. Moreover, the stability of proteins and their interactions in crowded macromolecular media are also intimately tied to the perturbations of the equilibrium polymer structure caused by the introduction of proteins [6–8].

Motivated by the above issues, many researches have examined the structure of flexible polymer solutions around spherical particles, and pertinent results have been obtained using a variety of analytical, numerical, and simulation methods [9–16]. In contrast to the situation for flexible polymers, much less theoretical advances have occurred in the more biologically and experimentally relevant context of mixtures of semiflexible or rodlike polymer solutions and spherical particles. Studies so far have only considered the behaviors of an isolated semiflexible polymer chain [17] and dilute solutions of rodlike polymers near spherical particles [18–21]. Scaling analysis and mean field theories have been presented for the structure of semiflexible polymer solutions and melts near flat surfaces [22–24]. To the best of our knowledge, there are no prior theoretical or numerical results which quantify the structure of semiflexible polymer solutions (at finite concentrations) near spherical particles.

This article presents a polymer self-consistent field theory based numerical analysis of the structure of semiflexible polymer solutions around spherical probes. We focus on the case where the polymers do not have any energetic interactions with the particle, and hence the model we consider is the case of a hard sphere inserted into a solution of semiflexible polymers. The polymers are expected to be depleted around the particle leading to an energetic cost of insertion of the particle. The present study is motivated by two issues.

(i) We desire to develop a fundamental understanding of the polymer concentration, polymer flexibility, and particle size dependencies of the insertion free energies of spherical probes in semiflexible polymer solutions. Indeed, many models for protein stability, partitioning and diffusion coefficients require knowledge of the insertion free energy and its scaling with sizes and concentrations [25–27]. We note in this regard that experiments which have examined properties such as the solubility of small particles in semiflexible polymer solutions have come to varied conclusions on their parametric dependcy upon the particle size R and polymer segment concentration ψ. Explicitly, quantities (P) such as solubility, insertion probability, and particle mobility (related to the exponential of the insertion free energy) have been described by functional forms [27–29]:

$$P = \exp(-\alpha R^{\beta}\psi^{\gamma}) \tag{1}$$

with the exponents $\beta \simeq 1-2$ and $\gamma \simeq 0.5-1$, and α a numerical constant. A clear explanation for the range of experimental results noted, and theoretical predictions for P does not exist. In this work we address this question explicitly and present numerically determined scaling laws which sheds light (at a mean-field level) on the range of exponents reported in experiments.

(ii) A second motivation for this article is to present a numerical apporach for the solution of the self-consistent field theory equations for semiflexible polymer solutions around spherical particles. SCFT equations for semiflexible polymers have been presented and numerically solved in ear-

*Author to whom correspondence should be addressed.

lier contexts relating to block copolymers [30], polymer solutions [31], and polymer melts near flat surfaces [24]. However, to our knowledge there has been no earlier work which has presented the numerical solution of the equations for situations embodying spherical symmetry. As we demonstrate later, spherical symmetry brings in some new features to the formulation and the resulting equations to be solved. We present the theoretical details and the numerical solution procedure for the resulting model. We note that with appropriate modifications, the formulation presented in this article may also be adapted for addressing the structural properties of isolated semiflexible polymers and their solutions confined in spherical geometries. We will address the latter issue in a subsequent article with special reference to its implications for DNA packaging problems.

The rest of this article is organized as follows. In Sec. I we present our model for semiflexible polymers, the formulation accounting for the spherical symmetry and the numerical solution procedure. The next two sections focus on the density profiles and the depletion thicknesses around a flat plate and a spherical particle. The results in the context of flat plates provide important insights on the different length scales and their interplay in determining the overall depletion thickness. We invoke physical arguments based on random phase approximation to extract numerical scaling laws describing the dependencies of the depletion thicknesses as a function of the different parameters. In the Sec. IV we present our results for insertion free energies of spherical particles and conclude with a few comments on the implications of our results for the context of the abovementioned experiments.

I. MODEL AND NUMERICAL DETAILS

A. Model and mean field limit

We consider a model for a solution of semiflexible polymers in the presence of a single spherical particle. We adopt a grand canonical formalism for the polymer solution and use the Kratky-Porod (KP) model to describe the conformations of the semiflexible polymers [32,33]. In the KP model, the polymer chains are represented by continuous space curves $R_i(s)$, where i indexes the different polymer chains and s denotes the arc length variable running from 0 to the contour length L. The bonded interactions in the KP model are quantified by an elastic bending energy of the form

$$\beta U_0 = \frac{\lambda}{2}\sum_{i=0}^{\infty}\int_0^L ds \left|\frac{d\mathbf{u}_i(s)}{ds}\right|^2, \tag{2}$$

where $\mathbf{u}(s)\equiv d\mathbf{R}/ds$ represents the tangent vector to the chain at the contour location s and is constrained to be a unit vector. λ represents the bending elasticity of the polymer, and is in turn directly proportional to its persistence length. To describe the excluded volume interactions between the different segments of the chain, we adopt the commonly used binary interaction model [34]:

$$\beta U_1 = \frac{v}{2}\sum_{i=0}^{\infty}\sum_{j=0}^{\infty}\int_0^L ds\int_0^L ds'\,\delta[\mathbf{R}_i(s)-\mathbf{R}_j(s')], \tag{3}$$

where $\delta(\cdots)$ represents the delta function enforcing locally the exclusion of overlaps of monomers, and v represents the strength of the excluded volume interactions.

In the grand canonical framework, the partition function of the polymer solution at an activity coefficient z_p can be expressed as [33,35]

$$\Xi(z_p,V,T) = \sum_{n=0}^{\infty}\frac{z_p^n}{n!}\int\prod_{i=1}^{n}d\mathbf{R}_i(s)\exp[-U_0-U_1] \times\prod_s\delta\left(\mathbf{u}_i(s)-\frac{d\mathbf{R}}{ds}\right)\delta[|\mathbf{u}_i(s)|-1]. \tag{4}$$

The above represents a functional integral over the different space curves $\mathbf{R}_i(s)$ statistically weighted by the Boltzmann factor corresponding to the energetic interactions U_0 and U_1. The first δ function above is used to enforce the constraint that $\mathbf{u}(s)$ represents the tangent vector at the chain at the location s, whereas the second delta function enforces the fact that $\mathbf{u}(s)$ is of magnitude unity. The above partition function can be transformed by using standard functional integral methods into a field theory where the fundamental degrees of freedom is a fluctuating potential field $w(\mathbf{r})$ [35]

$$\Xi = \int_{-i\infty}^{i\infty} Dw\,\exp\{-\beta H[w(\mathbf{r})]\}, \tag{5}$$

where

$$-\beta H[w(\mathbf{r})] = \frac{1}{2B}\int drw^2 + \frac{\alpha}{B}\int drw + Ze^{-\alpha}Q(w). \tag{6}$$

In the above, all length scales have been nondimensionalized by L. The constants $B\equiv vN^2/L^d$ and $Z\equiv z_pL^d$ represents the nondimensional excluded volume parameter and the activity coefficient of the polymer solution. The constant α satisfies $\alpha=BZ\exp(-\alpha)$, and is chosen so as to subtract out the free energy corresponding to a homogeneous polymer solution. Q represents the partition function of a single chain in the external potential field $w(\mathbf{r})$, and is given as

$$Q = \int q(\mathbf{r},\mathbf{u},1)d\mathbf{r}d\mathbf{u}, \tag{7}$$

where the field $q(\mathbf{r},\mathbf{u},s)$ satisfies the equation [32,33]

$$\frac{\partial q(\mathbf{r},s)}{\partial s} = -\mathbf{u}\cdot\nabla_{\mathbf{r}}q + \frac{1}{2\mu}\nabla_{\mathbf{u}}^2 q(\mathbf{r},s) - w(r)q,$$
$$q(\mathbf{r},\mathbf{u},s=0)=1. \tag{8}$$

Physically, $q(\mathbf{r},\mathbf{u},s)$ quantifies the statistical weight that a wormlike chain experiencing a potential $w(\mathbf{r})$ has its segment s at position $\mathbf{r}$ and with orientation $\mathbf{u}$. In the above equation, $\mu\equiv\lambda/N$ and represents the persistence length of the polymer expressed in units of the total contour length L. Using standard thermodynamic identities, the average homogeneous polymer solution density (nondimensionalized as C

$\equiv \psi L^d/N$) can be expressed in terms of the chemical potential Z as $C=Z\exp(-\alpha)$.

The polymer self-consistent field theory (SCFT) corresponds to a saddle point approximation of the above field theory [35]. In this framework, the integral over the potential field $w(\mathbf{r})$ in Eq. (5) is replaced by the value of the exponent evaluated at its saddle point. Explicitly, the saddle point field $w^*(\mathbf{r})$ is given as

$$w^*(\mathbf{r}) = BC[\phi(\mathbf{r}) - 1], \tag{9}$$

where the volume fraction field $\phi(\mathbf{r})$ is obtained from $q(\mathbf{r},\mathbf{u},s)$ as [33]

$$\phi(\mathbf{r}) = \frac{1}{4\pi}\int d\mathbf{u}\int_0^1 dsq(\mathbf{r},\mathbf{u},s;[w^*])q(\mathbf{r},-\mathbf{u},1-s;[w^*]). \tag{10}$$

Implementation of SCFT for different situations require the iterative solution of $w^*(\mathbf{r})$ which simultaneously satistifies Eqs. (9) and (10) [recall that $q(r,\mathbf{u},s)$ depends on $w(\mathbf{r})$ through Eq. (8)] subject to appropriate externally imposed constraints. In the specific case of polymer solutions near spherical particles, the influence of the particle is transformed as a boundary condition

$$q(r=R,\mathbf{u},s) = 0 \tag{11}$$

imposed on the surface of the sphere [8]. The self-consistent solution of Eqs. (8)–(11) then provides a mean-field approach to compute the grand canonical partition function $H[w^*(\mathbf{r})]$ and the polymer volume fraction profiles $\phi(\mathbf{r})$ as a function of the polymer chemical potential Z and the excluded volume parameter B. Knowledge of $\phi(\mathbf{r})$ allows us to determine an overall depletion thickness Δ defined as the equivalent radius of a shell over which a step function profile for the polymer density would be depleted [36]. In other words Δ is defined through

$$\frac{4\pi}{3}[(R+\Delta)^3 - R^3] = 4\pi\int_R^\infty drr^2[\phi(r)-1]. \tag{12}$$

B. Numerical solution procedure

In general, the diffusion equation (8) does not admit an analytical solution. For the limit $N\to\infty$, an approach termed as ground-state dominance allows one to simplify the equations and obtain analytical solutions for a few special cases [9,23]. Since our objective in this article is to examine the depletion characteristics for a range of particle sizes and concentration conditions, we resort to a numerical solution of Eq. (8). In solving Eq. (8) for polymer solution near a spherical particle, we exploit the fact that $q(\mathbf{r},\mathbf{u},s)$ possesses the symmetry

$$q(\mathbf{r},\mathbf{u},s) \equiv q(r,\mathbf{u}\cdot\mathbf{e}_r,s), \tag{13}$$

where r denotes the radial distance from the center of the sphere and $\mathbf{e}_r$ represents the unit radial vector (relative to an origin placed at the center of the sphere) at the location $\mathbf{r}$. By adopting a local coordinate system centered on $\mathbf{r}$ with $\mathbf{e}_r$ representing the Z axis and $\mathbf{u}\cdot\mathbf{e}_r=\cos\theta$, we can transform Eq. (8) as

$$\frac{\partial q(r,\theta,s)}{\partial s} = -\cos\theta\frac{\partial q}{\partial r} + \frac{\sin\theta}{r}\frac{\partial q}{\partial\theta} + \frac{1}{2\mu}\frac{1}{\sin\theta}\frac{\partial}{\partial\theta}\left(\sin\theta\frac{\partial q}{\partial\theta}\right) - w(r)q, \quad q(r,\theta,s=0)=1. \tag{14}$$

Equation (14) forms the starting point for analyzing the configurations of semiflexible polymers in situations embodying spherical symmetry. We note that a convenient way to solve Eq. (14) is by expanding $q(\mathbf{r},\theta,s)$ in Legendre polynomials as [37]

$$q(\mathbf{r},\theta,s) = \sum_l q_l(r,s)P_l(\cos\theta), \tag{15}$$

where P_l represents the lth order Legendre polynomial. By using the properties of P_l, equation (14) can be transformed as [37]

$$\frac{\partial q_l}{\partial s} = -\frac{l+1}{2l+3}\frac{\partial q_{l+1}}{\partial r} - \frac{l}{2l-1}\frac{\partial q_{l-1}}{\partial r} - \frac{(l+1)(l+2)}{2l+3}\frac{q_{l+1}}{r} + \frac{l(l-1)}{2l-1}\frac{q_{l-1}}{r} - \frac{l(l+1)}{2\mu}q_l - w(r)q_l, \tag{16}$$

subject to

$$q_l(r=R,s) = 0,$$

$$q_l(r,s=0) = \delta_{l,0}. \tag{17}$$

Moreover, Eq. (10) can be recast in terms of $q_l(r,s)$ as

$$\phi = \int_0^1 ds\sum_l\left[\frac{q_l(r,s)q_l^\dagger(r,1-s)}{2l+1}\right], \tag{18}$$

where $q_l^\dagger(r,s)$ satisfies

$$\frac{\partial q_l^\dagger}{\partial s} = \frac{l+1}{2l+3}\frac{\partial q_{l+1}^\dagger}{\partial r} + \frac{l}{2l-1}\frac{\partial q_{l-1}^\dagger}{\partial r} + \frac{(l+1)(l+2)}{2l+3}\frac{q_{l+1}^\dagger}{r} - \frac{l(l-1)}{2l-1}\frac{q_{l-1}^\dagger}{r} - \frac{l(l+1)}{2\mu}q_l^\dagger - w(r)q_l^\dagger, \tag{19}$$

subject to

$$q_l^\dagger(r=R,s) = 0,$$

$$q_l^\dagger(r,s=0) = \delta_{l,0}. \tag{20}$$

Our model is governed by three parameters: the nondimensionalized radius of the particle R, persistence length μ, the excluded volume parameter B, and the bulk concentration of the polymer C. As seen from the above equations, in the mean-field limit, the parameters B and C appear only as the combination BC in determining the density profiles $\phi(r)$. For the numerical results presented in the subsequent sections, we varied R (nondimensionalized by L) in the range 0.01–5, μ in the range 0.001–1, and BC in the range 0.01–100. This range of parameters allowed us to cover the regimes of particle sizes where R was the smallest length scale to the regime where the curvature of the particle was inconsequential.

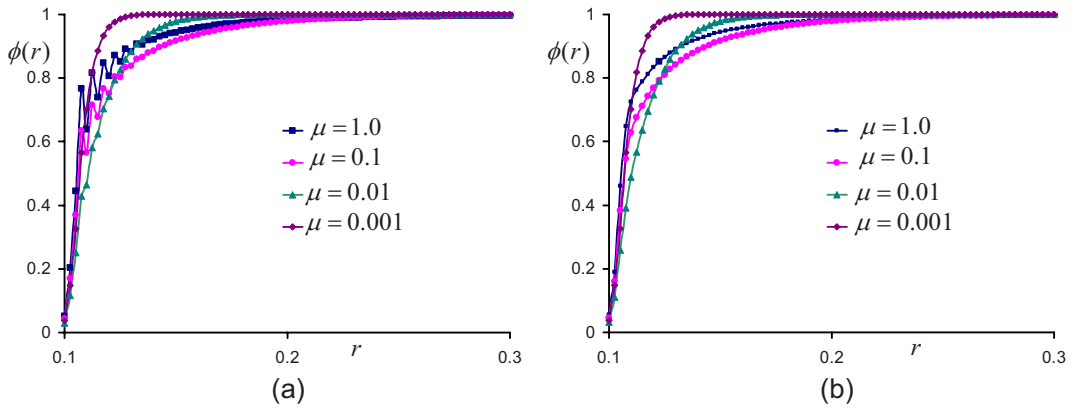

FIG. 1. (Color online) An illustration of the numerical issues and our procedure to resolve it. (a) Representative volume fraction profiles $\phi(r)$ for $R=0.1$ and μ values indicated in the figure. (b) Smoothed density profiles corresponding to the numerical results of (a).

Moreover, the range of μ chosen allowed us to span the regimes of flexible to rodlike polymers. The values of B and C covered the regimes ranging from dilute to concentrated polymer solutions.

The numerical results for $\phi(r)$ (methodology discussed below) are embedded within an iterative loop for determining the mean-field potential $w^*(\mathbf{r})$. The latter is accomplished by a real-space procedure identical to the one proposed by Fredrickson and Drolet [40], where $w_i^*(r)$, the guess for $w^*(\mathbf{r})$ at the ith step is evolved as

$$w_{i+1}^*(r) = w_i^*(r) + \epsilon\{BC[\phi(\mathbf{r}; w_i^*(r)) - 1] - w_i^*(r)\}. \quad (21)$$

An $\epsilon=0.005$ allowed us to attain convergence within few thousand iterations when starting from random initial conditions.

To obtain $\phi(r)$ for a given potential field $w_i^*(\mathbf{r})$, we solved equations (16) and (19) numerically by using a two-step Lax-Wenderoff (LW) method similar to the one suggested in Daoulas and co-workers [24,38]. Truncation of the Legendre polynomial expansion (15) at $l=12$ was found to ensure sufficient convergence of the density profiles. The presence of the discontinuous boundary condition at $r=R$ leads to numerical oscillations near the surface, which is a well-known artifact in the solution of hyperbolic partial differential equations [39]. To lucidate this, we display in Fig. 1(a) representative volume fraction profiles determined for radius $R=0.1$ and persistence lengths $\mu=0.001$, 0.01, 0.1, and 1.0. While the physical differences between the behaviors for these parameters constitute the focus of subsequent sections, the above discussed oscillations are certainly visible in the numerical results. We note that such artifacts become less pronounced for situations involving larger radii and/or smaller rigidity. Within the numerical schemes explored for this work, we were never able to completely eliminate such numerical oscillations. Instead, we adopted a two pronged strategy to account for such oscillations. (i) We used a one step Lax method close to the surface which is transitioned to the two step LW method [38]. (ii) We used a numerical smoothing procedure which averages out the oscillations to deduce a smooth variation in the density profile. We repeated the preceding steps with different discretizations to ensure numerical accuracy. The equations were typically solved by using a r discretization in the range $1-2.5\times10^{-3}$ and a $\delta s=1/2000$. The resulting density profiles were used to determine the depletion thicknesses which are discussed in the subsequent sections. In Fig. 1(b) we display the "smoothed" density plots corresponding to the original figures displayed in Fig. 1(a).

II. DEPLETION NEAR FLAT SURFACES

In this section, we present the numerical results for depletion thicknesses around large spherical objects and flat plates. In such a case, the polymer solution density profiles are independent of R and, hence,

$$\Delta_f = f(BC, \mu). \quad (22)$$

Shown in Fig. 2 are our numerical results for Δ_f displayed as a function of BC for different values of persistence lengths μ. We observe that at very low concentrations, the depletion thicknesses plateaus to a concentration independent value.

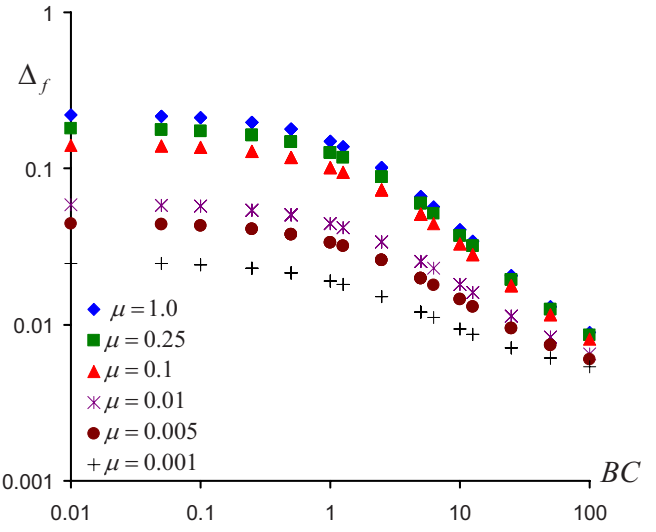

FIG. 2. (Color online) Depletion thicknesses Δ_f near flat plates as a function of the parameter BC for different persistence lengths μ.

Upon increasing the polymer concentrations, Δ_f is seen to decrease monotonically with concentration. Qualitatively, $\Delta_f(C\to 0)$ is expected to be representative of the size of an isolated semiflexible polymer chain, and hence, it is easy to understand that an increase in the rigidity of the polymer segments (the parameter μ) leads to a corresponding increase in the depletion thickness Δ_f. The influence of polymer concentrations can also be rationalized by noting that at higher concentrations the depletion thickness is expected to become related to the correlation length of density fluctuations in the polymer solution. The latter monotonically decreases with increasing polymer concentrations thereby explaining the behavior of the depletion thickness.

How do the quantitative details of the behavior observed in Fig. 2 compare with corresponding theoretical predictions? We first compare our numerical results $\Delta(C\to 0)$ with the theoretical prediction for the nondimensional size of a semiflexible polymer chain [41]

$$R_g(\mu) = \mu^{1/2}\left[\frac{1}{9} - \frac{\mu}{3} + \frac{2}{3}\mu^2 + \frac{2}{3}[-1+\exp(-1/\mu)]\mu^3\right]^{1/2}. \tag{23}$$

In Fig. 3(a), we compare $\Delta(C\to 0)$ alongside the above result, and observe that Eq. (23) provides an excellent fit to our results. This confirms our hypothesis that for dilute solutions, the depletion thickness is proportional to the size of the polymer chain and is given (the prefactor determined based on the fit to numerical data) as

$$\Delta_f(C\to 0) = 1.7\mu^{1/2}\left[\frac{1}{9} - \frac{\mu}{3} + \frac{2}{3}\mu^2 + \frac{2}{3}[-1+\exp(-1/\mu)]\mu^3\right]^{1/2}. \tag{24}$$

To understand quantitatively the origins of the concentration dependence of Δ_f, we note that for flexible polymer solutions, previous theoretical researches have confirmed that a correlation length derived based on random phase approximation (RPA) accurately models the mean-field concentration dependence of the depletion thickness near flat plates. Whence, it is of interest to compare our above results to the corresponding RPA predictions of correlation lengths for semiflexible polymer solutions ξ_{RPA}. Doi and co-workers considered the KP model for semiflexible polymers and derived a prediction for ξ_{RPA} as (in our notation and nondimensional variables) [41]

$$\xi_{\mathrm{RPA}} \propto R_g(\mu)(BC+1)^{-1/2}, \tag{25}$$

where $R_g(\mu)$ is given by Eq. (23). In Fig. 2(b), we compare the above with our numerical results by considering the ratio $\Delta_f/\Delta_f(C\to 0)$ [thereby normalizing the factor $R_g(\mu)$] as a function of BC. It is seen that that our numerical results are not consistent with the behavior expected for ξ_{RPA}. Explicitly, we observe for large μ the concentration decay is stronger than predicted, while for smaller persistence length μ the concentration decay is weaker than that expected for ξ_{RPA}. These results suggest that the depletion thicknesses exhibits a much more complex dependence on μ and BC than that

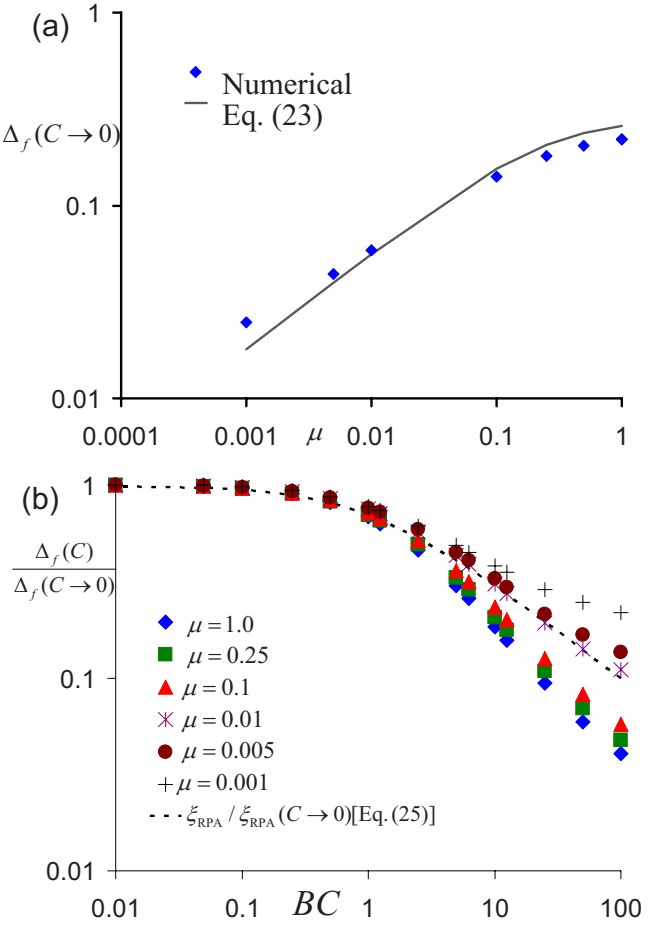

FIG. 3. (Color online) (a) A comparison of $\Delta_f(C\to 0)$ (displayed as points) with the theoretical predictions for the size of a semiflexible polymer chain (solid line). (b) $\Delta_f/\Delta_f(C\to 0)$ for polymer solutions of different persistence lengths. Dotted line represents the theoretical prediction for $\xi_{\mathrm{RPA}}/\xi_{\mathrm{RPA}}(C\to 0)$.

embodied in the RPA prediction for the correlation length ξ_{RPA}.

To gain more insight into the above discrepancies, we consider the RPA approximation for the density correlation function $g_{\mathrm{RPA}}(\mathbf{q})$ for semiflexible polymer solutions. While an exact expression for $g_{\mathrm{RPA}}(\mathbf{q})$ does not exist, approximate functional forms have been proposed in Marques and Fredrickson [42] and Netz *et al.* [43]. We adopt the results of Netz *et al.* which yields (in units of $\mathbf{q}$ normalized as $\mathbf{q}L$)

$$g_{\mathrm{RPA}}^{-1}(\mathbf{q}) = \frac{\alpha(\mu)q^2}{1+\alpha(\mu)q/\sqrt{6\pi}} + BC + 1, \tag{26}$$

where the function $\alpha(\mu)$ is given as

$$\alpha(\mu) = \mu\left[\frac{1}{9} - \frac{\mu}{3} + \frac{2}{3}\mu^2 + \frac{2}{3}[-1+\exp(-1/\mu)]\mu^3\right], \tag{27}$$

and is identical to the functional form for nondimensional $R_g^2(\mu)$ [Eq. (23)]. From Eq. (26) we deduce that

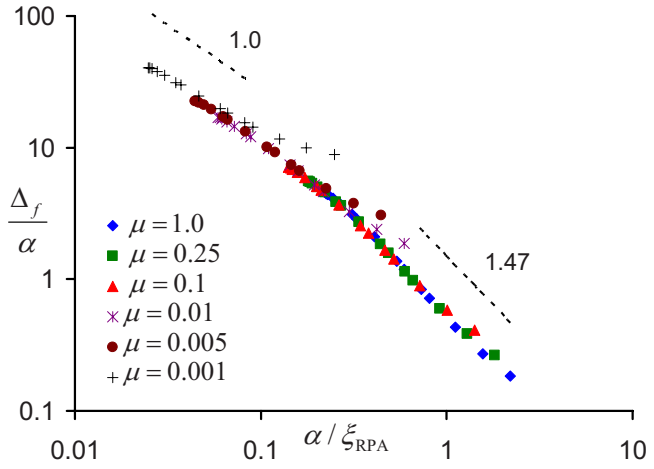

FIG. 4. (Color online) A test of the scaling proposal of Eqs. (29) and (30).

$$g_{\mathrm{RPA}}(\mathbf{q}) \sim \begin{cases} (q\sqrt{6\pi} + BC + 1)^{-1}, & q\alpha \gg 1, \\ (q^2\alpha + BC + 1)^{-1}, & q\alpha \ll 1. \end{cases} \tag{28}$$

From Eq. (28) it is evident that g_{RPA} is a function of three nondimensional length scales $\xi_{\mathrm{RPA}} \equiv \alpha(\mu)^{1/2}(BC+1)^{-1/2}$, $\alpha(\mu)$, and $(BC+1)^{-1}$. For $\alpha/\xi_{\mathrm{RPA}} < 1$, the decay behavior of g_{RPA} is dominated by $\xi_{\mathrm{RPA}} \equiv \alpha^{1/2}(\mu)(BC+1)^{-1/2}$. Using Eqs. (25) and (27) we observe that this regime occurs when the correlation length ξ_{RPA} is larger than the persistence length of polymer, which corresponds to the "flexible" limit of the semiflexible polymer solution. In such a case, we expect the depletion thickness to be closely related to ξ_{RPA}. In contrast, for $\alpha/\xi_{\mathrm{RPA}} > 1$ the decay behavior of g_{RPA} is determined by an interplay of the length scales ξ_{RPA} and $(BC+1)^{-1} \equiv \xi_{\mathrm{RPA}}^2/\alpha$. This regime ccurs for $\xi_{\mathrm{RPA}} \lesssim \mu$ or the "rigid" limit of the semiflexible polymer solution. In such a case, we might expect the depletion thickness also to reflect an interplay between the preceding two length scales.

The above reasoning can be encapsulated in a scaling proposal for the depletion thickness Δ_f as

$$\frac{\Delta_f}{\alpha} = f\left(\frac{\alpha}{\xi_{\mathrm{RPA}}}\right), \tag{29}$$

with $f(x)$ expected to behave as

$$f(x) \sim \begin{cases} x^{-1}, & x \ll 1, \\ x^{-2} & x \gg 1. \end{cases} \tag{30}$$

This hypothesis is tested in Fig. 4 by considering the ratio Δ_f/α as a function of $\alpha/\xi_{\mathrm{RPA}}$ [to ensure consistency, we used the numerical values for $\Delta_f(C \to 0)$ in place of $\alpha^{1/2}$]. It is observed that in the above representation, $f(x)$ exhibits a behavior of $x^{-0.97}$ for $x < 1$ which crosses over to $x^{-1.47}$ for $x > 1$. While we do not observe the crossover to the exponent -2 predicted for $x \gg 1$, we speculate that the transition from the exponent -1 to -1.47 is strongly suggestive of the crossover to the asymptotic scaling behavior and hence consider the numerical results in Fig. 4 to be in good agreement with the hypothesis and scaling predictions underlying Eq. (30).

In summary, our numerical results for the depletion of semiflexible polymers near flat objects suggests a complex interplay between the persistence length μ and the correlation length of the semiflexible polymer ξ_{RPA}. Explicitly, for the flexible limit of semiflexible polymers, we predict that the depletion thickness scales as the correlation length of the polymer solution. In contrast, for the limit of rigid polymers and rod solutions, our numerical results suggests that the density profiles exhibits an interplay between two length scales. Overall, this results in a scaling collapse of the depletion thickness as a function of the ratio $\alpha/\xi_{\mathrm{RPA}}$, and provides a quantitative prediction for use in experiments measuring the depletion thicknesses of semiflexible polymers near flat plates.

III. DEPLETION NEAR SPHERICAL OBJECTS

Next, we consider the depletion characteristics of semiflexible polymers around spherical objects which brings to fore an additional length scale, viz., the radius of the particle R. It is commonly supposed that for particle sizes R much larger than the flat plate depletion thickness Δ_f, curvature effects are negligible and that the depletion thickness around the spherical particles $\Delta_R \simeq \Delta_f$ [11]. The issue we address in this section is whether this consideration is indeed true for solutions of semiflexible polymers, and the implications of the persistence length-correlation length interplay noted in the preceding section. Due to numerical limitations however, we could only probe regimes such that $R/\Delta_f \geqslant 0.3$. Consequently, while we were able to address the relevance of curvature effects, our results do not allow us to draw concrete scaling conclusions regarding the behavior of depletion thicknesses for very small radii.

To render the parameter space tractable, we work in nondimensional variables. Explicitly, based on the parametric considerations discussed in the preceding section, we expect that

$$\Delta_R = f(BC, \mu, R). \tag{31}$$

Using the fact that Δ_f is a function of the parameters BC and μ, the above can be rewritten as

$$\Delta_R = f(\Delta_f, \mu, R). \tag{32}$$

Since we expect that the different quantities become independent of the contour length for large contour lengths, the above representation can be expressed in terms of three nondimensional combinations Δ_R/R, R/Δ_f, and R/μ as

$$\frac{\Delta_R}{R} = f\left(\frac{R}{\Delta_f}, \frac{R}{\mu}\right) \tag{33}$$

(we adopt this representation since it provides a better physical representation of some of the scaling collapses discussed below).

In Fig. 5 we display our numerical results for depletion thicknesses Δ_R/R as a function of R/Δ_f for different values of R/μ. To aid in the discussion, we have separated these results into three regimes:

(a) Figure 5(a) pertains to the results for $R/\Delta_f > 10$ and for the entire range of R/μ examined. It is seen that all the

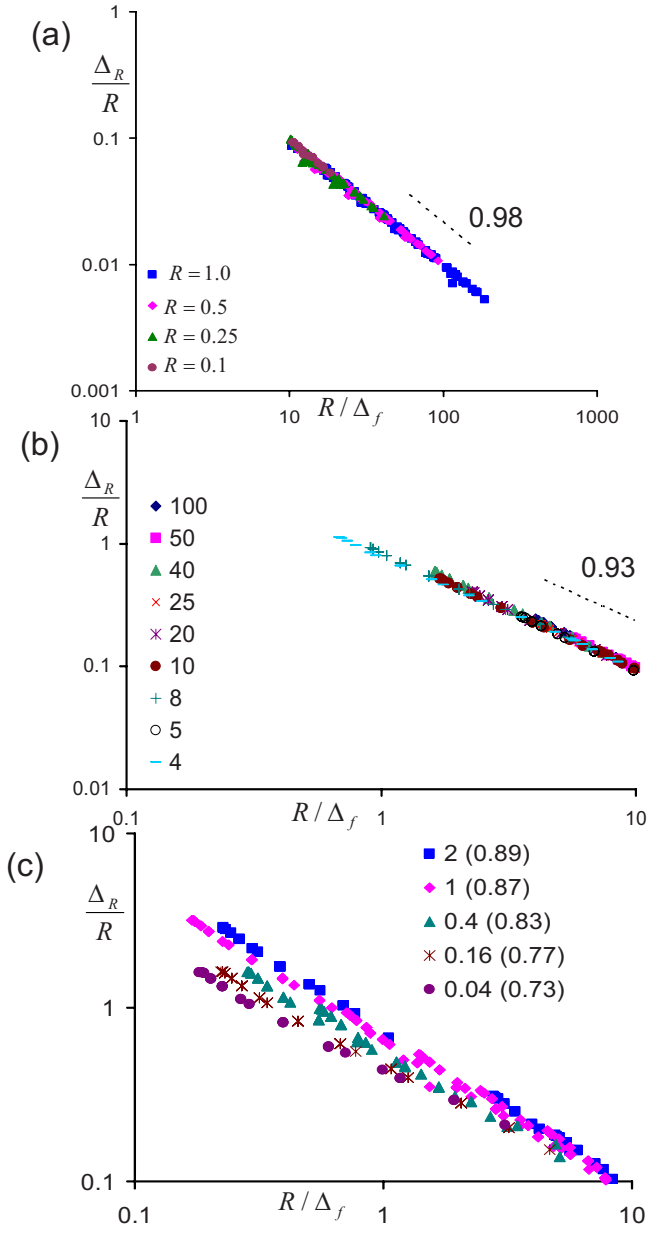

FIG. 5. (Color online) Depletion thicknesses Δ_R normalized by the radius R represented as a function of the depletion thicknesses near a flat plate (inversely normalized by R). (a) Numerical results for $R/\Delta_f > 10$ for different radii R and persistence lengths μ (to maintain clarity, we do not distinguish the different μ values by specific symbols). (b) Numerical results for $R/\Delta_f < 10$ for different R/μ indicated. (c) Numerical results for $R/\Delta_f < 10$ for different R/μ indicated. Numbers in the parenthesis correspond to the exponents of a power law fit of the data.

data for $R/\Delta_f > 10$ collapse onto a single curve which is independent of the value of R/μ and has a power-law slope of $\simeq -1$. This suggests that for this regime

$$\frac{\Delta_R}{R} \simeq \frac{\Delta_f}{R}, \tag{34}$$

or $\Delta_f \simeq \Delta_R$. This result reinforces the intuitive expectation that for very large particles (relative to the depletion thickness in the flat plate regime) the depletion thickness is independent of the curvature of the particles.

(b) Figure 5(b) displays the results of Δ_R/R for $0.3 < R/\Delta_f < 10$ for the regime $R/\mu \gtrsim 4$. We observe that our numerical results exhibit a scaling collapse of the form

$$\frac{\Delta_R}{R} \simeq \left(\frac{\Delta_f}{R}\right)^{-0.93}, \tag{35}$$

which is independent of the R/μ considered. Whence we conclude that for large values of R/μ, the curvature of the particles has only a small influence on the depletion thickness even upto the regime $R \simeq \Delta_f$ and

$$\Delta_R \simeq \Delta_f. \tag{36}$$

(c) Figure 5(c) displays the results of Δ_R/R for the regime $0.3 < R/\Delta_f < 10$ for the regime $R/\mu \lesssim 4$. In contrast to the behavior noted for larger values of R/μ, we observe that Δ_R/R now displays a strong dependence on the radius relative to the persistence length of the polymer. Explicitly, we observe that the Δ_R/R exhibits a scaling of the form

$$\frac{\Delta_R}{R} \simeq \left(\frac{R}{\Delta_f}\right)^{-\nu}, \tag{37}$$

with an exponent $\nu < 1$ (quantifying the deviation from the flat plate behavior), decreasing monotonically with lowering of R/μ. Moreover, it is seen that the radius at which the depletion thicknesses start to deviate from the flat plate regime also explicitly depends upon the ratio R/μ, with deviations observed at larger radii for smaller R/μ values.

A physical basis for the above trends can be obtained by combining the insights gleaned in the preceding section with the hypothesis that curvature effects manifest when the radius of the particles becomes comparable to length scales at which density variations occur near a flat plate. For the case where μ is small (the "flexible" limit of the semiflexible polymer), we suggested that the density profiles near a flat plate exhibit variations on a single length scale ξ_{RPA} and hence $\Delta_f \simeq \xi_{\mathrm{RPA}}$. In such regimes, curvature effects are also expected to occur only when $R \simeq \xi_{\mathrm{RPA}} \equiv \Delta_f$. Moreover, curvature effects are expected to be only a function of R/Δ_f and hence independent of the ratio R/μ (except insofar as the μ dependence embodied in Δ_f). This reasoning rationalizes the behavior noted in Fig. 5(b), where for large values of R/μ the curvature effects did not impact the depletion thickness up until the regime $R \simeq \Delta_f$, and the deviation from the flat plate scaling (an exponent of 0.93 versus an exponent of 1.0) was independent of R/μ.

In contrast, for larger μ (the rigid polymer limit), we suggested that the density profiles near a flat plate might exhibit a two length scale behavior which depends on ξ_{RPA} and $\xi_{\mathrm{RPA}}^2/\alpha(\mu)$ with Δ_f determined by their interplay [see Eq. (30)]. Since the density profiles exhibit variations on the length scale ξ_{RPA}, in this regime also we may expect curvature-induced deviations to begin when $R \simeq \xi_{\mathrm{RPA}}$. Since the length scales follow the hierarchy $\xi_{\mathrm{RPA}} > \Delta_f > \xi_{\mathrm{RPA}}^2/\alpha$, the curvature induced deviations occur for $R > \Delta_f$. Moreover, using Eq. (30) we have

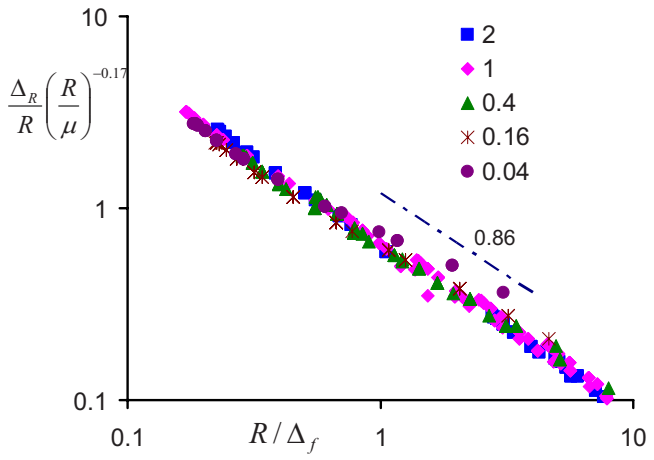

FIG. 6. (Color online) Empirical fit of Δ_R/R to the parameter $R/|\Delta_f$.

$$\frac{R}{\Delta_f} = \frac{R}{\xi}\left(\frac{\xi}{\alpha(\mu)}\right)^{\beta},$$

with $\beta<0$ ($\beta=-0.47$ in our numerical results, and expected to be -1 in the asymptotic scaling regime). When $R \simeq \xi$, we have

$$\frac{R}{\Delta_f} \simeq \left(\frac{R}{\alpha(\mu)}\right)^{\beta}. \tag{38}$$

Since $\alpha(\mu)$ is a monotonically increasing function of μ [see Eq. (27)], the above suggests that the curvature-induced deviations in this regime occur at larger values of R/Δ_f for systems with smaller values of R/μ. This reasoning rationalizes the behavior observed in Fig. 5(c), where indeed stronger deviations beginning at larger values of R/Δ_f where noted for systems with smaller R/μ values.

Due to the complex two parameter scaling expected for the regime depicted in Fig. 5(c), we are unable to propose a simple scaling collapse of the data. However, for the purposes of quantitative comparisons, we empirically fitted the data for $R/\mu \lesssim 2$ and extracted a power law profile of the form (fit displayed in Fig. 6):

$$\frac{\Delta_R}{R} \simeq \left(\frac{R}{\Delta_f}\right)^{-0.86}\left(\frac{R}{\mu}\right)^{0.17}, \quad 0.1 < R/\Delta_f < 10. \tag{39}$$

Considering the nonanalytic nature of the different exponents above, we speculate that the above scaling is not a manifestation of a distinct physical phenomena but rather a reflection of the crossover to the situation of very small particles. Unfortunately, due to numerical limitations we are unable to probe the latter regime to determine the precise asymptotic scaling laws.

In sum, our numerical results for the curvature dependence of the depletion thickness indicates novel behavior which sensistively depends on the persistence length of the polymer relative to the radius of the particle. For the case when the persistence length of the polymer is smaller than the radii, the depletion thickness was shown to exhibit very little curvature dependence, even for radii as small as R/Δ_f and $R/\xi_{\mathrm{RPA}} \simeq 0.5$. In contrast, for $R/\mu \lesssim 1$ and $R/\Delta_f \lesssim 10$, the depletion thickness starts to exhibit a curvature dependence for radii $R \simeq O(\mu)$, with the intensity of the curvature dependence monotonically increasing with an increase in the ratio μ/R.

The above results serve to higlight the subtleties in the depletion characteristics involving semiflexible polymers and small probes. Explicitly, the flexible limit is shown to behave quite differently from the rigid limit of the semiflexible polymers in their respective curvature dependencies of the depletion thickness (and correspondingly the free energies of insertion, as demonstrated in the next section). This revises the accepted wisdom that the curvature dependence of depletion thicknesses for polymer solutions occurs for particle sizes comparable to or smaller than the the depletion thicknesses for flat plates. Instead, we suggest that the such a notion is true only for solutions of flexible semiflexible polymers. In contrast, for rigid semiflexible polymer solutions, due to the disparity between the correlation length and the depletion thickness of the polymer solution, curvature effects manifest at a length scale much larger than the depletion thickness for flat plates.

IV. INSERTION FREE ENERGY

In this final section, we consider the dependence of the insertion free energy of the particles as a function of the different parameters in the system. As we will demonstrate, the insertion free energy of small particles is intimately tied to the depletion thickness Δ_R. Whence, the understanding developed in the preceding sections proves crucial in explaining the characteristics of the insertion free energies.

To deduce the insertion free energies, the free energy expression (6) is computed relative to the homogeneous solution for different parameters. The insertion free energy F_1 of a particle of size R can be expected to be expressed as [44]

$$F_1 = \Pi\frac{4}{3}\pi R^3 + 4\pi R^2\gamma. \tag{40}$$

In the above, the first term represents the volumetric energy contribution arising from the work needed to create a cavity of size R, and is expressed as the osmotic pressure of the solution Π multiplying the volume of the particle. For the mean-field situation considered in this article, we have for the nondimensionalized osmotic pressure

$$\frac{\Pi R_g^d}{k_B T} = C + \frac{BC^2}{2}, \tag{41}$$

and hence the parametric dependence of the first term in Eq. (40) can be considered as understood. The second term in Eq. (40) represents the energy penalty arising from the interfacial tension γ. The latter arises explicitly due to inhomogeneous density variations induced by the introduction of the particle, and is expected to dominate the insertion free energy for small particles.

In this section, we consider the numerical results for the interfacial tension term γ and rationalize our results by considering the explicit dependence of γ on the other parameters. Explicitly, we expect that for regimes where curvature

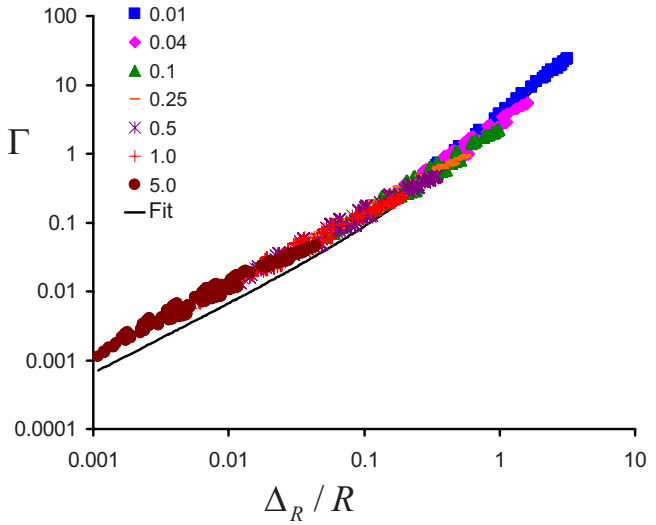

FIG. 7. (Color online) Numerical results for the normalized interfacial tension Γ as function of Δ_R/R for different radii. The results exihibit only little dependence on the specific μ values (chosen in the range 0.001–1). Hence, to maintain clarity we do not distinguish the different μ values in the plot. The above results are well-fit by an indicated quadratic function of the form $f(x)=0.65x+2.28x^2$.

effects do not play a significant role (see previous section), γ itself will be independent of R and only dependent on B, C, and μ. In contrast, we expect that in regimes where curvature effects manifest γ would also become dependent on the curvature in a manner similar to the Tolman corrections noted for the curvature dependence of surface tension for gas-liquid interfaces [44,45]. To render the analysis tractable, we again resort to a nondimensional framework, and nondimensionalize γ with the variable ΠR. Using $\Delta_R=f(BC,\mu,R)$, we expect

$$\Gamma \equiv \frac{\gamma}{\Pi R} = f\left(\frac{\Delta_R}{R}, \frac{\mu}{R}\right). \tag{42}$$

In Fig. 7 we display our results for Γ as a function of Δ_R/R for different radii. We observe that in this representation, the γ values collapse onto a single universal curve which is (practically) independent of the specific μ/R values. Moreover, we observe that the functional form of the curve can be well fit to a quadratic of the form

$$\Gamma = a\left(\frac{\Delta_R}{R}\right) + b\left(\frac{\Delta_R}{R}\right)^2, \tag{43}$$

where a and b are $O(1)$ constants determined by fitting our data. On physical terms, the above results can be understood based on the arguments used to motivate the nondimensionalization of γ. One way to think about the interfacial tension term is to think of it physically as the osmotic pressure contribution arising from the evacuation of polymers from a layer of thickness Δ_R surrounding the particle. For $\Delta_R<R$, we expect this energetic term to be of the form $4\pi R^2\Delta_R\Pi$, i.e., $\gamma \simeq \Delta_R\Pi$. These considerations lead to

$$\Gamma \simeq \frac{\Delta_R}{R}, \tag{44}$$

a functional form which is close to the result obtained by fitting our data. The second term in the fit of our numerical results can be understood as a manifestation of the curvature effects on γ which arises for the case when the depletion thicknesses become comparable to or larger than the radius of the particle.

We now discuss the implications of our results in the context of the experimental observations mentioned in the Introduction. Explicitly, our numerical results indicate that the insertion free energy for a spherical particle in a semiflexible polymer solution follows a functional relationship of the form

$$F_1 = \Pi\frac{4}{3}\pi R^3\left[1 + 1.95\frac{\Delta_R}{R} + 6.8\left(\frac{\Delta_R}{R}\right)^2\right] \text{ for } \frac{\Delta_R}{R} \leqslant 3.0. \tag{45}$$

It can be see that the size dependence of the insertion free energy exhibits a complex functional form which depends on R through through both the osmotic pressure and interfacial tension term. For large particles, the first term above is expected to dominate and the insertion free energy scales as R^3 and will exhibit a concentration dependence identical to that of the osmotic pressure. For smaller particles, the interfacial tension terms are expected to dominate and the insertion free energy is expected to be a function of Δ_R/R. In such a case, using the results discerned in Eqs. (29), (30), and (39) we can deduce that depending on the regime of values for Δ_R/R, F_1 can exhibit a particle size scaling dependence of the form R^β with β in the range 1–2. In a similar manner, the concentration dependence of the insertion free energy is also expected to exhibit a complex dependency on the parameters BC and μ whose functional form (not expressible as a simple power law) depends on the value of radius of the particle relative to the depletion thickness. These insights may serve to explain the different functional forms and exponents noted in the experimental literature regarding the solubility and mobility of small particles and proteins in semiflexible polymer solutions [27].

V. CONCLUSIONS AND OUTLOOK

In this article, we presented a numerical approach to the solution of the self-consistent field theory for the structure of semiflexible polymer solutions near spherical surfaces. We used the framework to study the depletion characteristics of semiflexible polymers near colloids and nanoparticles. Our results suggest that the depletion characteristics of semiflexible polymers exhibit more complex parametric dependencies than their flexible counterparts. Explicitly, the polymer density profiles (and the depletion thicknesses) were shown to be depend sensitively on the polymer concentrations, the persistence lengths and the radius of the particles. Broadly, two categories of features were identified based on the relative ratios of the persistence lengths to the correlation length of the polymer solution. For the flexible limit of semiflexible polymers, the correlation length proves to be the critical

length scale governing both the depletion thickness and the curvature effects. In contrast, for the rigid limit of the semiflexible polymer solutions the depletion thickness and the curvature effects were shown to be dependent on a length scale which was determined by an interplay between the persistence lengths and the correlation length. This led to nontrivial scaling laws governing the concentration and radii dependence of the depletion thicknesses. Our study also highlighted the manner in which the above features impact upon the insertion free energies of small probes in semiflexible polymer solutions.

Several directions present itself for future study. The framework presented in this article can be straightforwardly used to address the properties of confined semiflexible polymers and their solutions. As mentioned earlier, the results of such cases has attracted significant interest in the context of the DNA packaging context. Another extension of the present study would be to address the effect of attractive interactions between the polymer and probes. Such effects are bound to be of importance in biological contexts, and compared to the case of flexible polymers, the results for semiflexible polymers are still lacking.

ACKNOWLEDGMENTS

This work was supported in part by a grant from Robert A. Welch Foundation, the US Army Research Office under Grant No. W911NF-07-1-0268 and American Chemical Society Petroleum Research Fund grant. A part of this work was accomplished while one of the authors (V.G.) was on leave at the Indian Institute of Science, Bangalore.

[1] A. J. Levine and T. C. Lubensky, Phys. Rev. Lett. **85**, 1774 (2000).
[2] D. T. Chen, E. R. Weeks, J. C. Crocker, M. F. Islam, R. Verma, J. Gruber, A. J. Levine, T. C. Lubensky, and A. G. Yodh, Phys. Rev. Lett. **90**, 108301 (2003).
[3] B. S. Chae and E. M. Furst, Langmuir **21**, 3084 (2005).
[4] J. Y. Huh and E. M. Furst, Phys. Rev. E **74**, 031802 (2006).
[5] V. Pryamitsyn and V. Ganesan, Phys. Rev. Lett. **100**, 128302 (2008).
[6] D. Hall and A. P. Minton, Biochim. Biophys. Acta **1649**, 127 (2003).
[7] N. Kozer and G. Schreiber, J. Mol. Biol. **336**, 763 (2004).
[8] M. Surve, V. Pryamitsyn, and V. Ganesan, J. Chem. Phys. **122**, 154901 (2005).
[9] P.-G. de Gennes, *Scaling Concepts in Polymer Physics* (Oxford University Press, Oxford, 1979).
[10] P.-G. d. Gennes, C. R. Hebd. Seances Acad. Sci., Ser. A B, Sci. Math. Sci. Phys **288**, 359 (1979).
[11] J. F. Joanny, L. Leibler, and P. G. De Gennes, J. Polym. Sci., Polym. Phys. Ed. **17**, 1073 (1979).
[12] E. J. Meijer and D. Frenkel, Phys. Rev. Lett. **67**, 1110 (1991).
[13] T. Odijk, Macromolecules **29**, 1842 (1996).
[14] A. Hanke, E. Eisenriegler, and S. Dietrich, Phys. Rev. E **59**, 6853 (1999).
[15] M. Fuchs and K. S. Schweizer, J. Phys.: Condens. Matter **14**, R239 (2002).
[16] A. A. Louis, P. G. Bolhuis, E. J. Meijer, and J. P. Hansen, J. Chem. Phys. **117**, 1893 (2002).
[17] R. R. Netz and J. F. Joanny, Macromolecules **32**, 9026 (1999).
[18] Y. Mao, P. Bladon, H. N. W. Lekkerkerker, and M. E. Cates, Mol. Phys. **92**, 151 (1997).
[19] Y. Mao, M. E. Cates, and H. N. W. Lekkerkerker, J. Chem. Phys. **106**, 3721 (1997).
[20] Y. L. Chen and K. S. Schweizer, J. Chem. Phys. **117**, 1351 (2002).
[21] Y. L. Chen and K. S. Schweizer, Langmuir **18**, 7354 (2002).
[22] D. W. Schaefer, J. F. Joanny, and P. Pincus, Macromolecules **13**, 1280 (1980).
[23] A. N. Semenov, Europhys. Lett. **9**, 353 (2002).
[24] K. C. Daoulas, D. N. Theodorou, V. A. Harmandaris, N. C. Karayiannis, and V. G. Mavrantzas, Macromolecules **38**, 7134 (2005).
[25] N. L. Abbott, D. Blankschtein, and T. A. Hatton, Macromolecules **24**, 4334 (1991).
[26] E. W. Merrill, K. A. Dennison, and C. Sung, Biomaterials **14**, 1117 (1993).
[27] B. Amsden, Macromolecules **31**, 8382 (1998).
[28] K. Luby-Phelps, Curr. Opin. Cell Biol. **6**, 3 (1994).
[29] R. J. Phillips, W. M. Deen, and J. F. Brady, AIChE J. **35**, 1761 (1989).
[30] M. W. Matsen, J. Chem. Phys. **104**, 7758 (1996).
[31] A. J. Spakowitz and Z. G. Wang, J. Chem. Phys. **119**, 13113 (2003).
[32] N. Saito, K. Takahashi, and Y. Yunoki, J. Phys. Soc. Jpn. **22**, 219 (1966).
[33] G. H. Fredrickson, *The Equilibrium Theory of Inhomogeneous Polymers* (Clarendon Press, Oxford, 2006).
[34] M. Doi and S. Edwards, *The Theory of Polymer Dynamics* (Oxford University Press, Oxford, 1986).
[35] G. Fredrickson, V. Ganesan, and F. Drolet, Macromolecules **35**, 16 (2002).
[36] G. J. Fleer, A. M. Skvortsov, and R. Tuinier, Macromolecules **36**, 7857 (2003).
[37] J. D. Jackson, *Classical Electrodynamics* (Wiley, New York, 1975).
[38] W. H. Press, B. P. Flannery, S. A. Teukolsky, and W. T. Vetterling, *Numerical Recipes in C: The Art of Scientific Computing*, 2nd ed. (Cambridge University Press, Cambridge, 1992).
[39] R. J. LeVeque, *Numerical Methods for Conservation Laws* (Birkauser-Verlag, Basel, 1992).
[40] F. Drolet and G. H. Fredrickson, Phys. Rev. Lett. **83**, 4317 (1999).
[41] T. Shimada, M. Doi, and K. Okano, J. Chem. Phys. **88**, 7181 (1988).
[42] C. M. Marques and G. H. Fredrickson, J. Phys. II **7**, 1805 (1997).
[43] P. Friedel, A. John, D. Pospiech, D. Jehnichen, and R. R. Netz, Macromol. Theory Simul. **11**, 785 (2002).
[44] A. A. Louis, P. G. Bolhuis, E. J. Meijer, and J. P. Hansen, J. Chem. Phys. **116**, 10547 (2002).
[45] J. S. Rowlinson, *Molecular Theory of Capillarity* (Clarendon Press, Oxford, 1982).